

DOI: [10.29026/oea.2024.230184](https://doi.org/10.29026/oea.2024.230184)

Tailoring electron vortex beams with customizable intensity patterns by electron diffraction holography

Pengcheng Huo^{1†}, Ruixuan Yu^{1†}, Mingze Liu¹, Hui Zhang¹,
Yan-qing Lu^{1,2*} and Ting Xu^{1,2*}

An electron vortex beam (EVB) carrying orbital angular momentum (OAM) plays a key role in a series of fundamental scientific researches, such as chiral energy-loss spectroscopy and magnetic dichroism spectroscopy. So far, almost all the experimentally created EVBs manifest isotropic doughnut intensity patterns. Here, based on the correlation between local divergence angle of electron beam and phase gradient along azimuthal direction, we show that free electrons can be tailored to EVBs with customizable intensity patterns independent of the carried OAM. As proof-of-concept, by using computer generated hologram and designing phase masks to shape the incident free electrons in the transmission electron microscope, three structured EVBs carrying identical OAM are tailored to exhibit completely different intensity patterns. Furthermore, through the modal decomposition, we quantitatively investigate their OAM spectral distributions and reveal that structured EVBs present a superposition of a series of different eigenstates induced by the locally varied geometries. These results not only generalize the concept of EVB, but also demonstrate an extra highly controllable degree of freedom for electron beam manipulation in addition to OAM.

Keywords: electron vortex beam; orbital angular momentum; diffraction holography

Huo PC, Yu RX, Liu MZ et al. Tailoring electron vortex beams with customizable intensity patterns by electron diffraction holography. *Opto-Electron Adv* 7, 230184 (2024).

Vortices widely exist on all scales in nature, such as gravitational vortices around black holes in universe, typhoon vortices on earth and quantum vortices in super-fluids. Among them, quantum vortices are particularly interesting because they can be represented by free movement of a single particle, which was first proposed by Allen et al. in 1992¹. It was discovered that an optical vortex beam with integer topological charge l can carry a quantized orbital angular momentum (OAM) $l\hbar$ per

photon (where \hbar is the reduced Planck's constant). This discovery unveiled a new understanding of the connection between macroscopic optical phenomenon and quantum mechanism²⁻⁷. The quantized OAM of photon offers a new degree of freedom of light and has significantly broadened the avenues of application including optical trapping^{8,9}, high-resolution microscopy^{10,11} and information processing¹²⁻¹⁴.

As another important elementary particle, electrons

¹National Laboratory of Solid-State Microstructures and Collaborative Innovation Center of Advanced Microstructures, Nanjing University, Nanjing 210093, China; ²College of Engineering and Applied Sciences, Key Laboratory of Intelligent Optical Sensing and Manipulation and Jiangsu Key Laboratory of Artificial Functional Materials, Nanjing University, Nanjing 210093, China.

[†]These authors contributed equally to this work.

*Correspondence: YQ Lu, E-mail: yqlu@nju.edu.cn; T Xu, E-mail: xuting@nju.edu.cn

Received: 23 October 2023; Accepted: 25 December 2023; Published online: 26 February 2024



Open Access This article is licensed under a Creative Commons Attribution 4.0 International License.

To view a copy of this license, visit <http://creativecommons.org/licenses/by/4.0/>.

© The Author(s) 2024. Published by Institute of Optics and Electronics, Chinese Academy of Sciences.

have drawn considerable attention in the fields from electron microscopy to nanofabrication. Different from massless neutral photons, electrons are massive charged particles and obey Fermi-Dirac statistics. In spite of this, electrons can still be represented by waves and free-electron wave functions. As a result, similar to photons, electrons are also able to be shaped to produce electron vortex beam (EVB) carrying OAM. In 2010, EVB was first generated by using spiral phase plates consisting of spontaneously stacked graphite thin films to impart OAM onto the incident electron beam¹⁵. Thereafter, several approaches, such as employing holographic masks^{16–19}, magnetic lens aberrations²⁰ and magnetic needles²¹, are reported to generate EVBs. Because EVB can effectively interact with matter as well as with external electric and magnetic fields, it is now starting to find applications as nanoscale magnetic probes for characterizing materials^{22,23}.

Thus far, all the experimentally generated EVBs with integer topological charge exhibit isotropic doughnut intensity patterns. One approach to break the isotropy is to introduce a fractional topological charge^{24,25}, which would consistently generate C-shaped EVBs. Actually, a few of early studies in optics suggest that the intensity pattern of vortex structure can be engineered on-demand by introducing nonuniformity into the phase gradient around the central singular point^{26,27}. Here, we generalize the concept of EVBs and present an experimental generation of structured EVBs in free-space. By designing and fabricating nanoscale holographic masks to shape the incident free electrons in the transmission electron microscope (TEM), three structured EVBs with identical OAM are engineered to exhibit customizable and completely different intensity patterns. Furthermore, based on the modal decomposition, we quantitatively investigate the OAM spectral distributions of structured EVBs and reveal that, although macroscopically the structured EVBs can be quantified and characterized by a single integer that describes the global topological invariance, which is similar to the ordinary ones, microscopically they present a superposition of a series of different eigenstates induced by the locally varied geometries. As the structured EVBs simultaneously have two independent controllable degree of freedom for electron beam manipulation including topological charge and intensity pattern, we envision this work may open new frontiers in related fundamental research and technical application of particle physics.

In principle, a free-space EVB is formed by continuous phase distributions around the center singularity that can be evaluated as the loop integral of the phase gradient in the transverse plane²⁸,

$$\oint_C \nabla \varphi \cdot d\mathbf{s} = 2\pi l, \quad (1)$$

where φ is the phase, \mathbf{s} is the unit vector tangential to the closed path C , and l is the topological charge. Ordinarily, the phase of EVB uniformly varies following a circular path around the vortex center and can be simply expressed as $l\theta$ (θ is azimuthal angle). Here, for generalizing the definition of EVB, we rewrite the wave function of EVB as $\Psi = Ae^{if(\theta)}$, where A is the amplitude, and $f(\theta)$ is parameterized azimuthal angle under constraint condition $f(2\pi) - f(0) = 2\pi$. The phase gradient $\partial\varphi/\partial\theta = lf'(\theta)$ is no longer a constant but a function varying along the azimuthal direction. According to the ray theory, the local divergence angle of the electron beam is proportional to the phase gradient $lf'(\theta)$ (see Supplementary information Section 1 for more details). Therefore, for a given topological charge l , the modulated electron beam would evolve into a structured vortex in the far-field with the geometry same as the contour of the parameterized azimuth gradient $f'(\theta)$. In other words, through deliberately designing the trajectory of $f'(\theta)$ in polar coordinates, the structured EVB is expected to exhibit desired intensity distribution. As proof-of-concept, herein we employ computer-generated hologram and design binary phase masks to demonstrate the creation of three types of structured EVBs, including a clover EVB with three-fold rotational symmetry, a non-closed spiral EVB and a custom arrowhead EVB, as illustrated in Fig. 1.

Figure 2(a–c) show the calculated parameterized azimuth gradients $f'(\theta)$ for these three structured EVBs. For the clover EVB and spiral EVB, $f'(\theta)$ are given by $f_1'(\theta) = 1 + \cos(3\theta)/2$ (Fig. 2(a)) and $f_2'(\theta) = 1 - \cos(\theta/2)/2$ (Fig. 2(b)), respectively. For more complex structured EVB with unformulated pattern, such as the custom arrowhead vortex beam proposed here, $f_3'(\theta)$ can be presented by the Fourier series expansion (see Supplementary section 2 for more details). Through integration of $f'(\theta)$ and then multiplying topological charge l , we can obtain the desirable parameterized phase profile φ_1 , φ_2 and φ_3 (Fig. 2(d–f)), which will be used to shape the incident free electrons and generate the corresponding structured EVBs. Based

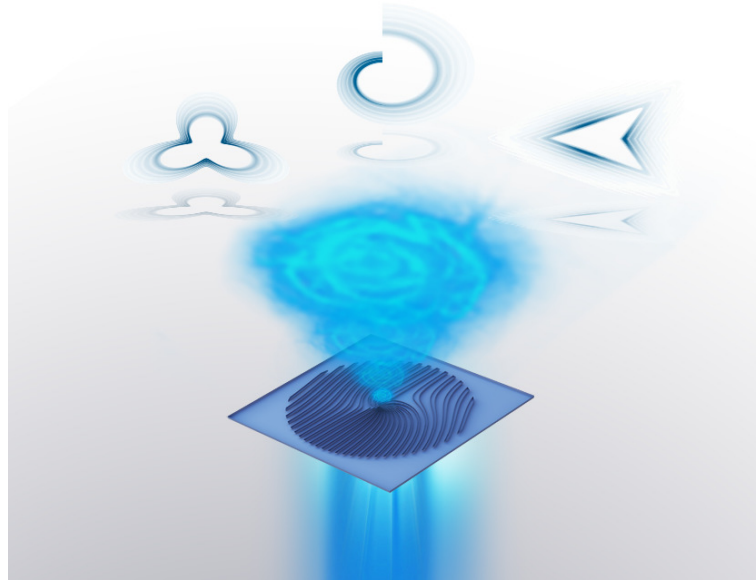


Fig. 1 | Schematic of the generation of structured EVBs. The binary holographic phase masks can be engineered with the generalized spiral phase to shape the incident free electrons to generate structured EVBs with customizable intensity patterns. The phase mask is composed of nanoscale forked gratings fabricated on 100 nm-thick silicon nitride membranes.

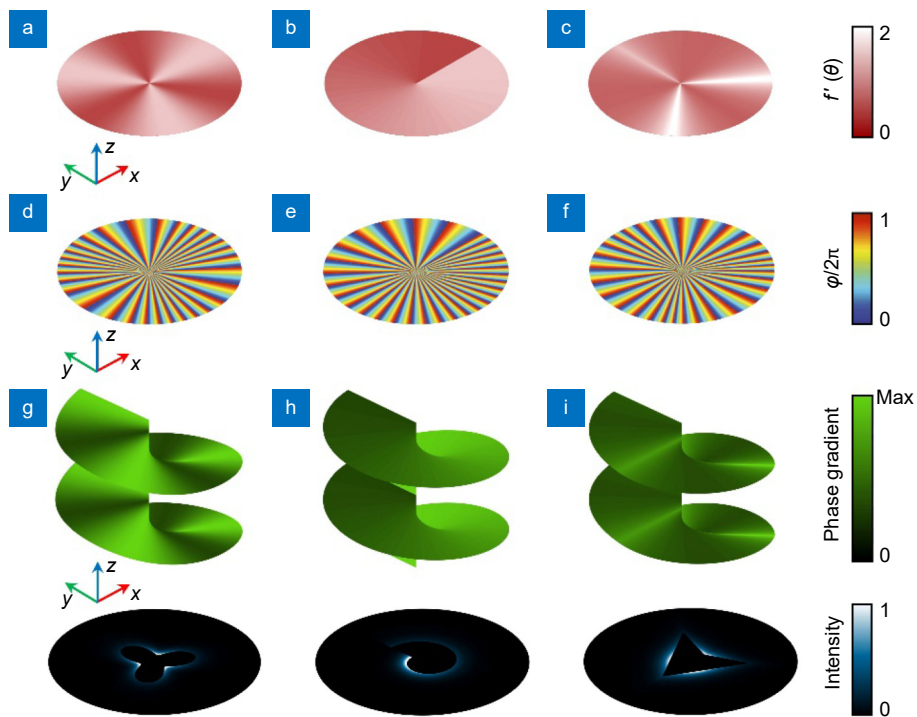


Fig. 2 | Theoretical construction of structured EVBs. (a–c) Three parameterized azimuth gradients $f_1'(\theta)$, $f_2'(\theta)$ and $f_3'(\theta)$, corresponding to the patterns of clover, spiral and arrowhead, respectively. (d–f) Desired generalized spiral phase of three EVBs ϕ_1 , ϕ_2 and ϕ_3 with identical topological charge $l = 30$. (g–i) Calculated wavefronts and intensity distributions of three structured EVBs.

on these results, Fig. 2(g–i) present the calculated wavefronts and intensity distributions of three structured EVBs with identical topological charge $l = 30$. Different from the ordinary helical wavefront of EVB with a constant phase gradient, the helical wavefronts of structured

EVBs exhibit non-uniformly distributed phase gradients. As expected, the calculated intensity distributions in the far-field reveal three EVBs exactly exhibit clover, spiral and arrowhead intensity patterns.

In experiment, we fabricate binary holographic phase

masks composed of nanoscale forked gratings to create the structured EVBs. The phase masks can be imprinted with desired phase shift by adjusting the thickness of electron-transparent material^{29–31}. Here, a transverse composite phase profile φ , which is the superposition of a generalized spiral phase and a Bragg carrier phase, imparts to the phase masks (see Supplementary Section 3 for more details). The additional Bragg carrier phase term can separate different diffraction orders and avoid crosstalk between them when electron beams pass through the grating masks. Corresponding to three structured EVBs mentioned above, the fabricated phase masks on 100 nm-thick Si_3N_4 membranes by focused-ion beam (FIB) milling are shown in Fig. 3(a–c). Each mask is etched in a circular area with a diameter $d = 15 \mu\text{m}$, and the grating is designed with a periodicity $p = 150$

nm. The enlarged insets of the fabricated masks show clear feature of the fork dislocations which indicates the encoded topological charge $l = 30$.

When illuminated with free electrons, the phase masks can impart the predesigned phase front onto the electron wave packets at the first order of diffraction, which would form the structured EVBs in the far-field. These generated EVBs are captured at the focal plane of magnetic lens system in the TEM. Figure 3(d–f) show the experimentally recorded images of the diffracted electron waves through the phase masks (+1 diffraction order), which clearly show clover, spiral and arrowhead intensity patterns, respectively. The electron phase maps, acquired by using the defocus series reconstruction technique based on the Gerchberg-Saxton transmission iterative algorithm (see Supplementary information Section

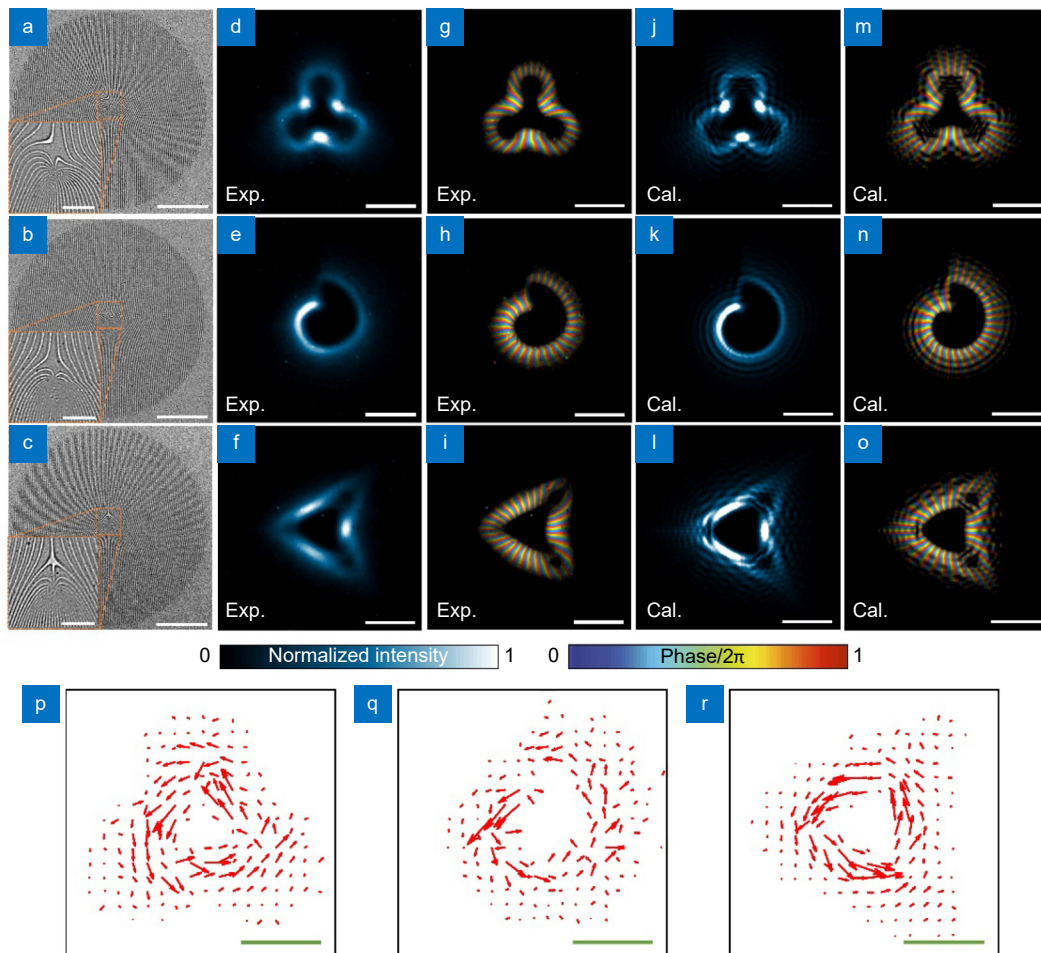


Fig. 3 | Experimental generation of structured EVBs using nanoscale holographic phase masks with fork dislocations. (a–c) The scanning electron microscope (SEM) images of phase masks for three EVBs. Scale bars: $4 \mu\text{m}$. Insets are the enlarged middle portions of phase masks. Scale bars: $1 \mu\text{m}$. (d–f) Experimentally recorded far-field intensity distributions and (g–i) Phase profiles retrieved by the transmission iterative algorithm. (j–l) Calculated far-field intensity distributions and (m–o) phase profiles. Scale bars of (d–o): $3 \mu\text{rad}$. (p–r) In-plane components of the probability current density vectors of three EVBs extracted from experimental measurements. The red arrows indicate the direction of the probability current of electron. The lengths of the red arrows are given in arbitrary unit normalized to the maximum value. Scale bars of (p–r): $3 \mu\text{rad}$.

4 for more details), are given in Fig. 3(g–i). The phase distributions show that the modulated electron beams have a $2\pi l$ azimuthal phase swirl in free-space, which confirms their vortex features. These experimental results match very well with the calculated ones those are obtained by Fourier transform on the corresponding binary phase distributions (Fig. 3(j–o)). Additionally, in order to quantitatively analyze the geometries of the structured EVBs, the diffraction angle distributions are also experimentally measured. Owing to a relatively constant focal length of the Fourier transform lens during the measurements, the diffraction angle can be conveniently used as a substitute for the radial distance in the intensity pattern of EVBs. As shown in Supplementary information Fig. S4, the measured diffraction angle distributions are consistent with the theoretical predictions.

To better understand the physical picture of structured EVB, we further investigate the probability current density in quantum electron states, defined as $\mathbf{j} = \hbar \text{Im}(\psi^* \nabla \psi) / m$, where m is mass of a nonrelativistic electron and wave function ψ can be described by amplitude and phase²³. According to its definition, the probability current density can reflect the local phase gradient in an arbitrary electron field, and thus is very suitable to characterize the angular momentum property of a free-space electron wave function. Figure 3(p–r) present the in-plane components of the experimentally measured probability current density vectors of three structured EVBs. For each case, although the current density is nonuniformly distributed, it follows the gradient of the electron phase and produces an effective loop of charge current, and thus forms a vortex around the beam axis. These results agree well with the calculated ones shown in Supplementary information Fig. S5. The probability current density can be further used to calculate the average electron OAM via the following volume integration: $\langle L_z \rangle = m \left| \int \boldsymbol{\rho} \times \mathbf{j} dV \right| / \left(\int \psi^* \psi dV \right)$, where $\boldsymbol{\rho}$ is the radial coordinates. For these three EVBs, the corresponding average OAM per electron are obtained as $28.1\hbar$, $28.3\hbar$ and $28.6\hbar$, respectively, which are all close to the expectation OAM corresponding to the imparted topological charge $l = 30$. Moreover, based on modal decomposition approach, we quantitatively analyze the OAM spectral distributions of three structured EVBs (see Supplementary information Section 5 for details). By projecting the wave function into the helical harmonics of different orders, the weight factor of each intrinsic OAM mode is obtained, as shown in Fig. 4. In contrast to

ordinary EVBs, the OAM modes of structured EVBs span a large spectral range, which indicates that they present as a superposition of a series of eigenstates. Therefore, although these structured EVBs have almost identical average OAM, their locally varied geometries lead to completely different spectral distributions.

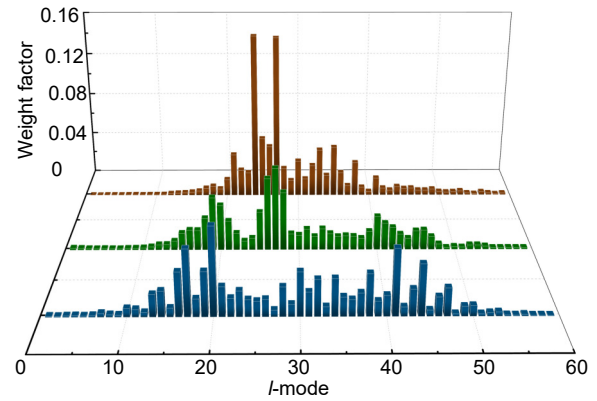


Fig. 4 | Modal decomposition of EVBs. The OAM spectral distributions of three structured EVBs extracted from the experimental results. The blue, green and red histograms correspond to clover, spiral and arrowhead EVBs, respectively.

In addition to generation, we also investigate the coherent superposition of two structured EVBs with different topological charges of l_1 and l_2 . The morphology of phase masks designed for creating superposed states of structured EVBs are determined by the product of two transmission phase functions respectively corresponding to l_1 and l_2 . For each type of structured EVB, we fabricate phase mask simultaneously imparted with topological charge $l_1 = 30$ and $l_2 = 33$, as shown in Fig. 5(a–c). The experimentally recorded transverse intensity distributions of three states are shown in Fig. 5(d–f). In spite of different intensity distributions, all the superposed states clearly exhibit petal-like interference patterns with exactly 3 lobes, which are consistent with the calculated results (Fig. 5(g–i)). This demonstration verifies that although microscopically structured EVBs consist of a range of discrete OAM modes, the coherent superposition state of two structured EVBs still depends on their global topological invariances and thus yields interference pattern with $|l_1 - l_2|$ petals, behave similarly as the unstructured ones.

In summary, we have developed a nanoscale platform for generating and manipulating structured EVBs in free-space. By designing the generalized spiral phases and imparting them onto the incident free electrons, we experimentally demonstrate that EVBs can be engin-

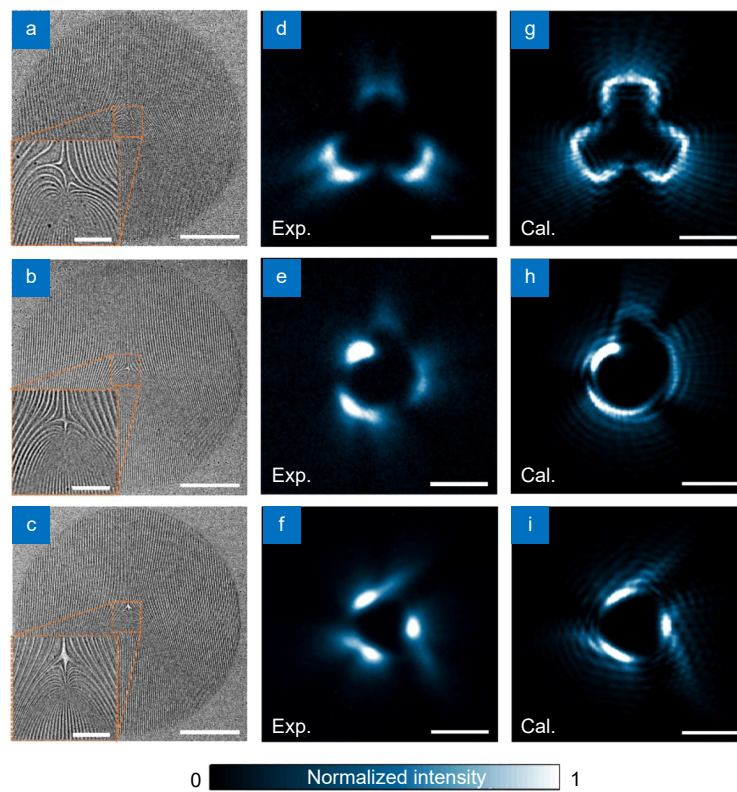


Fig. 5 | Coherent superposition of structured EVBs. (a–c) The SEM images of fabricated phase masks to generate superposition states of topological charge $l_1 = 30$ and $l_2 = 33$, corresponding to three structured EVBs. Scale bars: 4 μm . Insets are the enlarged middle portions of phase masks. Scale bars: 1 μm . (d–f) Experimentally recorded interference patterns of the superposition states. (g–i) Simulated interference patterns of superposition states. Scale bars of (d–i): 3 μrad .

eered with different intensity patterns. Unlike classic vortices, the orbital motions of structured EVBs are not attributed to the collective behavior of many electrons, and no external field or force are necessary for the generation. Thanks to its additional controllable degree of freedom, the structured EVB as a quantum electron probe holds great potential in electron microscopy³² and can further promote various *in-situ* applications, such as electron manipulation of nanoparticles along designed trajectories³³, pattern-dependent interaction of electron OAM with matter³⁴ and selectively exciting and probing surface plasmon modes^{35,36}. The structured EVBs also can be directly used in lithography to produce shaped nanostructures without the need to scan the beam. Moreover, such concept and generation approach are convenient to generalize to other particle systems, such as neutron³⁷, proton³⁸, atom and molecule^{39,40}.

Methods

Sample preparation

In this work, the binary phase masks are fabricated on 100 nm-thick silicon nitride membranes by using focused-ion-beam (FIB) milling. The FIB tool utilizing Ga-

ions is operated at acceleration voltage of 30 keV and beam current of 7.7 pA. The patterning is performed with a minimum step size of 4 nm and a dwell time of 0.42 ms.

TEM measurement

The evolution of electron vortex is observed in a Tecnai TF20 field emission gun TEM, which produces a coherent monoenergetic electron beam with an energy of 200 keV, corresponding to the relativistic de Broglie wavelength of approximately ~ 2.51 pm. The phase masks are placed at the front focal plane of the magnetic lens. When illuminated with coherent electron beam, the phase mask can shape the electron wave packets to form structured EVBs in the back focal plane of magnetic lens system. The diffraction patterns are recorded using low angle diffraction (LAD) mode, for which the magnetic lens is operated at low current. The LAD mode enables long camera length, so the diffractive angles for electrons < 1 μrad can be measured. A charge-coupled device (CCD) camera is used to capture the propagation dynamics of the generated EVBs.

References

- Allen L, Beijersbergen MW, Spreeuw RJC, Woerdman JP. Orbital angular momentum of light and the transformation of Laguerre-Gaussian laser modes. *Phys Rev A* **45**, 8185–8189 (1992).
- Pu MB, Li X, Ma XL, Wang YQ, Zhao ZY et al. Catenary optics for achromatic generation of perfect optical angular momentum. *Sci Adv* **1**, e1500396 (2015).
- Shen YJ, Wang XJ, Xie ZW, Min CJ, Fu X et al. Optical vortices 30 years on: OAM manipulation from topological charge to multiple singularities. *Light Sci Appl* **8**, 90 (2019).
- Fang XY, Ren HR, Li KY, Luan HT, Hua YL et al. Nanophotonic manipulation of optical angular momentum for high-dimensional information optics. *Adv Opt Photonics* **13**, 772–833 (2021).
- Guo YH, Zhang SC, Pu MB, He Q, Jin JJ et al. Spin-decoupled metasurface for simultaneous detection of spin and orbital angular momenta via momentum transformation. *Light Sci Appl* **10**, 63 (2021).
- Zhang YX, Liu XF, Lin H, Wang D, Cao ES et al. Ultrafast multi-target control of tightly focused light fields. *Opto-Electron Adv* **5**, 210026 (2022).
- Porfirev A, Khonina S, Ustinov A, Ivliev N, Golub I. Vectorial spin-orbital Hall effect of light upon tight focusing and its experimental observation in azopolymer films. *Opto-Electron Sci* **2**, 230014 (2023).
- Paterson L, MacDonald MP, Arlt J, Sibbett W, Bryant PE et al. Controlled rotation of optically trapped microscopic particles. *Science* **292**, 912–914 (2001).
- Grier DG. A revolution in optical manipulation. *Nature* **424**, 810–816 (2003).
- Willig KI, Rizzoli SO, Westphal V, Jahn R, Hell SW. STED-microscopy reveals that synaptotagmin remains clustered after synaptic vesicle exocytosis. *Nature* **440**, 935–939 (2006).
- Luo XG. Principles of electromagnetic waves in metasurfaces. *Sci China Phys, Mech Astron* **58**, 594201 (2015).
- Nicolas A, Veissier L, Giner L, Giacobino E, Maxein D et al. A quantum memory for orbital angular momentum photonic qubits. *Nat Photonics* **8**, 234–238 (2014).
- Ren HR, Li XP, Zhang QM, Gu M. On-chip noninterference angular momentum multiplexing of broadband light. *Science* **352**, 805–809 (2016).
- Fang XY, Ren HR, Gu M. Orbital angular momentum holography for high-security encryption. *Nat Photonics* **14**, 102–108 (2020).
- Uchida M, Tonomura A. Generation of electron beams carrying orbital angular momentum. *Nature* **464**, 737–739 (2010).
- Verbeeck J, Tian H, Schattschneider P. Production and application of electron vortex beams. *Nature* **467**, 301–304 (2010).
- McMorran BJ, Agrawal A, Anderson IM, Herzing AA, Lezec HJ et al. Electron vortex beams with high quanta of orbital angular momentum. *Science* **331**, 192–195 (2011).
- Grillo V, Gazzadi GC, Mafakheri E, Frabboni S, Karimi E et al. Holographic generation of highly twisted electron beams. *Phys Rev Lett* **114**, 034801 (2015).
- Yuan XY, Xu Q, Lang YH, Jiang XH, Xu YH et al. Tailoring spatiotemporal dynamics of plasmonic vortices. *Opto-Electron Adv* **6**, 220133 (2023).
- Petersen TC, Weyland M, Paganin DM, Simula TP, Eastwood SA et al. Electron vortex production and control using aberration induced diffraction catastrophes. *Phys Rev Lett* **110**, 033901 (2013).
- Béché A, Van Boxem R, Van Tendeloo G, Verbeeck J. Magnetic monopole field exposed by electrons. *Nat Phys* **10**, 26–29 (2014).
- Harris J, Grillo V, Mafakheri E, Gazzadi GC, Frabboni S et al. Structured quantum waves. *Nat Phys* **11**, 629–634 (2015).
- Bliokh KY, Ivanov IP, Guzzinati G, Clark L, Van Boxem R et al. Theory and applications of free-electron vortex states. *Phys Rep* **690**, 1–70 (2017).
- Mousley M, Thirunavukkarasu G, Babiker M, Yuan J. Robust and adjustable C-shaped electron vortex beams. *New J Phys* **19**, 063008 (2017).
- Yang YQ, Forbes A, Cao LC. A review of liquid crystal spatial light modulators: devices and applications. *Opto-Electron Sci* **2**, 230026 (2023).
- Freund I. Optical vortices in Gaussian random wave fields: statistical probability densities. *J Opt Soc Am A* **11**, 1644–1652 (1994).
- Freund I, Freilikh V. Parameterization of anisotropic vortices. *J Opt Soc Am A* **14**, 1902–1910 (1997).
- Nye JF, Berry MV. Dislocations in wave trains. *Proc Roy Soc A Math Phys Eng Sci* **336**, 165–190 (1974).
- Harvey TR, Pierce JS, Agrawal AK, Ercius P, Linck M et al. Efficient diffractive phase optics for electrons. *New J Phys* **16**, 093039 (2014).
- Grillo V, Karimi E, Gazzadi GC, Frabboni S, Dennis MR et al. Generation of nondiffracting electron Bessel beams. *Phys Rev X* **4**, 011013 (2014).
- Polman A, Kociak M, Javier García de Abajo F. Electron-beam spectroscopy for nanophotonics. *Nat Mater* **18**, 1158–1171 (2019).
- Yu RX, Huo PC, Liu MZ, Zhu WQ, Agrawal A et al. Generation of perfect electron vortex beam with a customized beam size independent of orbital angular momentum. *Nano Lett* **23**, 2436–2441 (2023).
- Verbeeck J, He T, Van Tendeloo G. How to manipulate nanoparticles with an electron beam. *Adv Mater* **25**, 1114–1117 (2013).
- Lloyd S, Babiker M, Yuan J. Quantized orbital angular momentum transfer and magnetic dichroism in the interaction of electron vortices with matter. *Phys Rev Lett* **108**, 074802 (2012).
- Ugarte D, Ducati C. Controlling multipolar surface Plasmon excitation through the azimuthal phase structure of electron vortex beams. *Phys Rev B* **93**, 205418 (2016).
- Guzzinati G, Béché A, Lourenço-Martins H, Martin J, Kociak M et al. Probing the symmetry of the potential of localized surface plasmon resonances with phase-shaped electron beams. *Nat Commun* **8**, 14999 (2017).
- Clark CW, Barankov R, Huber MG, Arif M, Cory DG et al. Controlling neutron orbital angular momentum. *Nature* **525**, 504–506 (2015).
- Madan I, Vanacore GM, Gargiulo S, LaGrange T, Carbone F. The quantum future of microscopy: wave function engineering of electrons, ions, and nuclei. *Appl Phys Lett* **116**, 230502 (2020).
- Lembessis VE, Ellinas D, Babiker M, Al-Dossary O. Atom vortex beams. *Phys Rev A* **89**, 053616 (2014).
- Luski A, Segev Y, David R, Bitton O, Nadler H et al. Vortex beams of atoms and molecules. *Science* **373**, 1105–1109

(2021).

Acknowledgements

This work is supported in part by the Key Research and Development Program from Ministry of Science and Technology of China (2022YFA1205000), National Natural Science Foundation of China (12274217 and 62105142), Natural Science Foundation of Jiangsu Province (BK20220068 and BK20212004) and Fundamental Research Funds for Central Universities. The authors acknowledge the technique support from the microfabrication center of the National Laboratory of Solid-State Microstructures (NLSSM).

Author contributions

P. C. Huo, R. X. Yu, M. Z. Liu and H. Zhang performed the theoretical design, numerical simulations, and experimental measurements. All authors contributed toward the interpretation of results and participated in manuscript preparation. Y. Q. Lu and T. Xu directed the project.

Competing interests

The authors declare no competing financial interests.

Supplementary information

Supplementary information for this paper is available at <https://doi.org/10.29026/oea.2024.230184>



Scan for Article PDF